PCCP

Cite this: *Phys. Chem. Chem. Phys.*, 2012, **14**, 2791–2796

www.rsc.org/pccp

PAPER

Phase diagram and structural evolution of Ag–Au bimetallic nanoparticles: molecular dynamics simulations

Sang Chul Yeo, Da Hye Kim, Kihyun Shin and Hyuck Mo Lee*

Received 11th November 2011, Accepted 4th January 2012
DOI: 10.1039/c2cp23547a

We studied the structural evolution of a 270-atom Ag–Au bimetallic nanoparticle (2 nm in size) with varying composition and temperature. The liquid to solid transition region and the solid-state structure were investigated using molecular dynamics simulations. To determine the exact transition temperature region, we applied the mean square displacement and structure deviation methods, as well as the generally used caloric curve of potential energy *versus* temperature. The results showed that a complete solid–solution phase diagram of the binary Ag–Au system was obtained. Irrespective of the composition, the freezing temperature of a Ag–Au bimetallic nanoparticle was lower than that of the bulk state by a margin of several hundred degrees, and three different solid-state structures are proposed in relation to the Au composition. Our phase diagram offers guidance for the application of Ag–Au nanoparticles.

Introduction

Bimetallic nanoparticles have received considerable attention from the scientific community because of their unique physical and chemical properties.[1–7] Nanoparticles generally possess different properties from bulk materials as a result of their large surface-to-volume ratio. Melting temperature depression is one of their well-known properties. In the past few decades, many experiments have provided theoretical evidence of melting temperature depression, but the experiments consumed an immense amount of time and effort.[8–10] Recently, there has been a steady increase in interest in the catalytic role of bimetallic nanoparticles. In particular, Ag–Au bimetallic nanoparticles have attracted considerable attention. They are the most optical of all bimetallic nanoparticles, are harmless and environmentally friendly,[11–15] and they have excellent catalytic properties.[14–17] Generally, Au nanoparticles can be used in many selective oxidation reactions.[18–20] One way of improving the ability of Au to activate oxidation is to alloy it with Ag. Ag nanoparticles are also a catalyst for CO oxidation, but they require a higher temperature than Au. Some research groups have consequently investigated the improved synergistic effects of the Ag–Au bimetallic system. Iizuka *et al.* found that Ag impurities in unsupported Au nanoparticles enhance their catalytic activity in CO oxidation.[20,21] Wang *et al.* reported that the Ag–Au bimetallic system has good catalytic activity on a mesoporous support for CO oxidation.[14,22–24] They experimentally investigated the high catalytic activity with an Ag/Au ratio of 0.37 : 1 in an Ag–Au bimetallic catalyst supported on TiO_2. They successfully synthesized nanoparticles with various Ag/Au atomic ratios.[14,22,25]

A phase diagram presents information on the phase stability of multicomponent bulk materials with respect to temperature and composition. Because the properties of nanoscale materials are different from those of bulk materials, a separate phase diagram is needed for nanoparticles.[26,27] A theoretical method called the computer coupling of phase diagrams and thermochemistry (CALPHAD) is generally used to predict and produce phase diagrams.[8,28] However, the CALPHAD method is reported to have a size limitation: the radius of the particles must be greater than approximately 5 nm.[28–30] Molecular dynamics (MD) simulation is another useful way of producing phase diagrams.[26,31] In this study, we performed MD simulations with a cooling process to produce a nano phase diagram of 2 nm size Ag–Au bimetallic nanoparticles with various compositions. Our analysis determined the exact transition temperature and transition region, as well as the details of the temperature-dependent structural evolution of each composition. Our results for various bimetallic compositions confirm the overall structural stabilization during the cooling process.

Computational details

We performed classical MD simulations under NVT conditions with XMD code.[32,33] The quantum Sutton–Chen many-body potential was used.[34–36] We applied a fifth-order Gear predictor–corrector algorithm with a time step of 1 fs to solve Newton's dynamic equation.[37] We prepared Ag–Au bimetallic nanoparticles consisting of 270 atoms (2 nm in size) with a composition range of 10 at% to 90 at%, incremented by 10 at%.

Department of Materials Science and Engineering, KAIST, 291 Daehak-ro, Yuseong-gu, Daejeon, 305-701, Republic of Korea. E-mail: hmlee@kaist.ac.kr; Fax: +82-42-350-3310; Tel: +82-42-350-3334

The bimetallic nanoparticles were placed in the center of a large simulation box (1000 A × 1000 A × 1000 A). The Ag–Au bimetallic nanoparticles were fully annealed at 1000 K to exclude the effect of their initial configuration on the phase transition temperature; then, they were cooled to 300 K at a cooling rate of 10 K ns^{-1}. We also performed the same simulations at the various cooling rates of 5 K ns^{-1}, 20 K ns^{-1}, and 40 K ns^{-1} to consider the dependence on the cooling rate. The liquid to solid transition temperatures changed little with the cooling rate. However, at the cooling rates of 20 K ns^{-1} and 40 K ns^{-1}, there was not enough time to stabilize the 270 atom Ag–Au bimetallic nanoparticles and the different structural transformation was observed. Rossi and Ferrando[38] and Shibuta and Suzuki[39] reported the same trend in the structural transformation of Au and Ag nanoparticles, respectively, with the cooling rate. The slow cooling rate equal to or below 10 K ns^{-1} seems reasonable in this study.

An important step in the production of the nano phase diagram was the determination of the liquid to solid transition temperature region. For all of the compositions, we used the widely accepted caloric curve of potential energy *versus* temperature. We were generally able to find the liquid to solid transition region with a simulated annealing method by observing the rapid reduction in the caloric curve of the potential energy or the total energy *versus* temperature. However, the caloric curve alone is sometimes insufficient to determine the exact freezing or melting temperature (for example, in the case of the glass transition) because the potential energy does not change abruptly in this case.[40] Thus, we adopted the mean square displacement (MSD) and structural deviation (SD) analysis methods. These additional methods are useful for finding the exact freezing transition temperature and numerically predicting the structural evolution.

Mean square displacement

The MSD method is generally used to analyze the dynamic properties of materials.[41–43] We can compare and determine the variation of the diffusion coefficients to determine whether a nanoparticle is in a solid state or a liquid state. We calculated the MSD as follows:

$$\mathrm{MSD} = \langle r^2(t) \rangle = \left\langle \frac{1}{N} \sum_{i=0}^{N} (r_i(t) - r_i(0))^2 \right\rangle \qquad (1)$$

where N is the total number of atoms; $r_i(t)$ is the position of atom i at each step; $(r_i(t) - r_i(0))$ is the distance traveled by atom i over a time interval, t; and $(r_i(t) - r_i(0))^2$ is the mean square displacement of each step. Using MSD analysis, we determined the phase transition temperature from the steep change in the MSD value. The movement of atoms depends on the phase state of the material; therefore, we can easily identify the phase transition region with MSD analysis.

Structural deviation

The SD method can determine the extent of dispersion from the average potential energy per time step. This method is a supplement to the caloric curve, similar to MSD, in that it can distinguish between the transition from liquid to crystalline and the transition from liquid to amorphous. We calculated the SD as follows:

$$\mathrm{SD} = \sqrt{E[(X - \mu)^2]} \qquad (2)$$

where the operator E is the average value of the potential energy X and μ is the mean value of the potential energy for each temperature. The sharp peaks in the SD curve are expected to correspond to the temperatures at which there is an observable drop in the potential energy because of the liquid to solid transition. This SD method of identifying the phase transition temperature is similar to the heat capacity method. We can use the SD method to distinguish whether the phase transition is induced by a liquid-to-crystalline or liquid-to-amorphous (glass) transition.

Results and discussion

Fig. 1 shows the caloric curve (potential energy *vs.* temperature) of Ag–Au bimetallic nanoparticles for each composition in the range of 10 at% to 90 at%, which was varied in increments of 10 at%. These results are used to estimate the rapid reduction of the potential energy, which indicates the occurrence of a liquid to solid transition. As shown in Fig. 1, the caloric curves of all of the bimetallic compositions are divided into two types: Type 1 and Type 2. The main distinguishing feature of the two types is the exactitude of the transition temperature. Type 1 includes the Ag-rich compositions of Ag90Au10, Ag80Au20 and Ag70Au30; this transition type is indicative of a phase transition from liquid to glass. In such cases, the exact transition temperature is difficult to determine. Our results confirm that the transition from the liquid state to the solid state occurs during the overall cooling process, and the final structure is similar to an amorphous (disordered) structure. A Type 2 transition exhibits a distinct transition temperature from liquid to solid. The Ag60Au40, Ag50Au50, Ag40Au60, Ag30Au70, Ag20Au80, and Ag10Au90 compositions exhibit Type 2 transitions. Type 2 can be further divided into two cases based on further investigation of their solid structures at room temperature: Case 1 and Case 2. These cases are based on aspects of their structural evolution. As indicated in Table 1, Case 1 refers to transformations to an icosahedron (Ih) structure with fivefold symmetry, and Case 2 refers to transformations to a crystalline (FCC) structure.

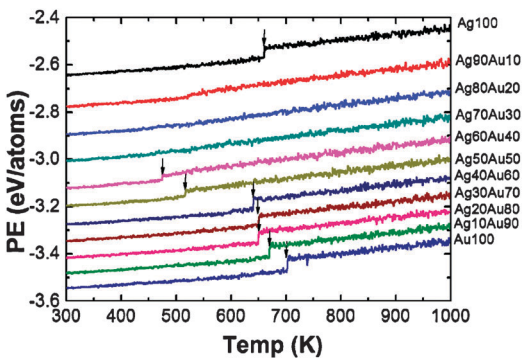

Fig. 1 Caloric curve of Ag–Au bimetallic nanoparticles for all compositions. Arrows indicate the solidification temperature. PE is the potential energy.

Table 1 Transition temperature and transition range of each composition (0, 10…100 at% Au) together with the transformation types

	(L–S) Transition temperature			
Composition	T_L/K	T_S/K	ΔT/K	Transformation types
Ag100	640	630	10	L → crystal (Ih)
Ag90Au10	560	520	40	L → amorphous structure
Ag80Au20	560	455	105	L → amorphous structure
Ag70Au30	580	490	90	L → amorphous structure
Ag60Au40	485	480	5	L → crystal (Ih)
Ag50Au50	520	515	5	L → crystal (Ih)
Ag40Au60	640	635	5	L → crystal (FCC)
Ag30Au70	650	645	5	L → crystal (FCC)
Ag20Au80	655	650	5	L → crystal (FCC)
Ag10Au90	675	665	5	L → crystal (FCC)
Au100	700	690	10	L → crystal (FCC)

T_L: surface freezing temperature. T_S: full freezing temperature.

Case 1 includes the pure Ag nanoparticles, while Case 2 includes the pure Au nanoparticles.

As mentioned, the Type 1 phase transition temperature (Ag-rich composition) is difficult to determine from a caloric curve of the potential energy alone, which changes monotonically. We therefore applied the MSD and SD methods. Because Type 1 has an unclear transition temperature as shown in Fig. 1, the MSD method was used to determine the exact temperature. As shown in Fig. 2(a), the MSD of Ag90Au10 produced three regions with different slopes (although the differences in slope were not conspicuous), and the transition was found to occur in the range of 520 K to 560 K. For the Ag40Au60, Ag30Au70, Ag20Au80, and Ag10Au90 compositions, the MSD behaved like a step function, as shown in Fig. 2(b). The transition temperatures were easy to detect. The SD curve confirms the nature of the transition from the liquid state, to either a crystalline structure or an amorphous one. The key factor in this determination is the presence of a specific peak in the SD results.[40,44,45] No specific peak was observed in Fig. 2(c) for Ag90Au10, Ag80Au20 or Ag70Au30. In these compositions, the structure was confirmed to be amorphous rather than crystalline. In contrast, the liquid-to-crystalline transition exhibited a sharp peak upon cooling, as can be seen in Fig. 2(d). Compositions that underwent this transition include Ag40Au60, Ag30Au70, Ag20Au80 and Ag10Au90. Table 1 summarizes the results of the three analysis methods with respect to the observed transition temperatures and transition regions for all compositions.

For the Type 2 compositions, the same solid state structures were not observed. In experimental terms, the structure of pure Ag was found to be icosahedral rather than crystalline (FCC).[46,47] According to the study by Baletto and Ferrando, Ag liquid nanodroplets tend to produce an Ih structure during the freezing of nanoparticles (for a number of atoms $245 \leq N \leq 310$).[48] When we calculated the single point energy of the Ag-Ih and Ag-FCC, the Ag-Ih (2 nm size) was more stable than the Ag-FCC by approximately 1.5 eV. In contrast, the experimental results for pure Au show that the FCC structure is more stable than the Ih structure. Nam *et al.* investigated Au nanoclusters; they found that the freezing phase was followed by the formation of ordered nanosurfaces with a fivefold symmetry, which ultimately led to the formation of an Ih structure.[49,50] The final structures were Ih for Case 1 and FCC for Case 2. According to the Ferrando group, pure Ag (2 nm size) is more stable with an Ih structure, and pure Au is more stable with a crystalline (FCC) structure.[51] We performed MD simulations to investigate the structural transformation in both Case 1 (Ih) and Case 2 (FCC). In particular, we tried to determine how the nanoparticle size affects the ground state structure of the pure Ag and pure Au nanoparticles. The results showed that the Ih structure is favored by pure Ag nanoparticles of up to 820 atoms (3 nm size) and by pure

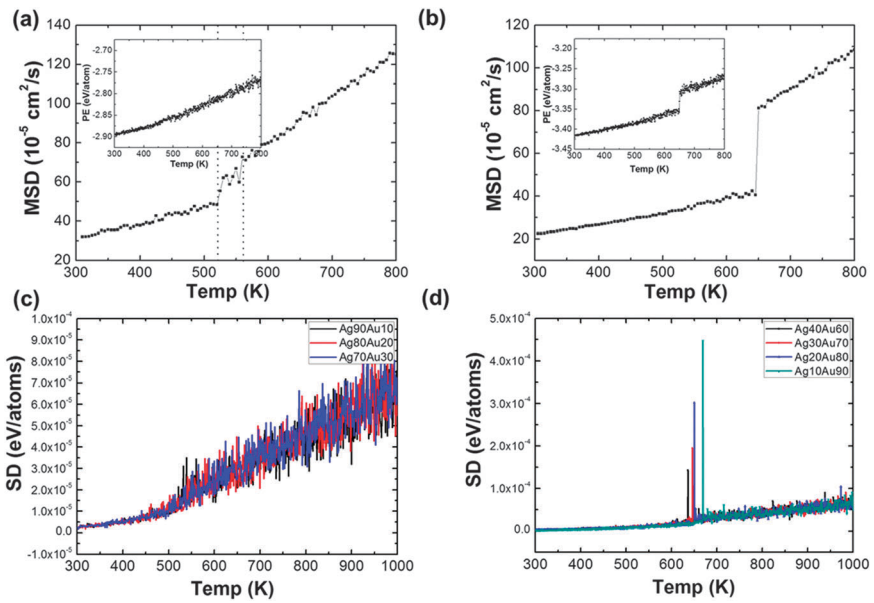

Fig. 2 (a) MSD curve of Ag90Au10 composition, indicating a smooth transition; the caloric curve (inset) is indicative of a glass transition, (b) MSD curve of Ag20Au80 composition showing a steep liquid to solid transition, (c) SD curve of Ag90Au10, Ag80Au20, Ag70Au30 compositions indicating glass transition from liquid to amorphous (without any noticeable specific peak) and (d) SD plot of Ag40Au60, Ag30Au70, Ag20Au80, Ag10Au90 compositions showing sharp peaks corresponding to the start of the liquid to solid transition.

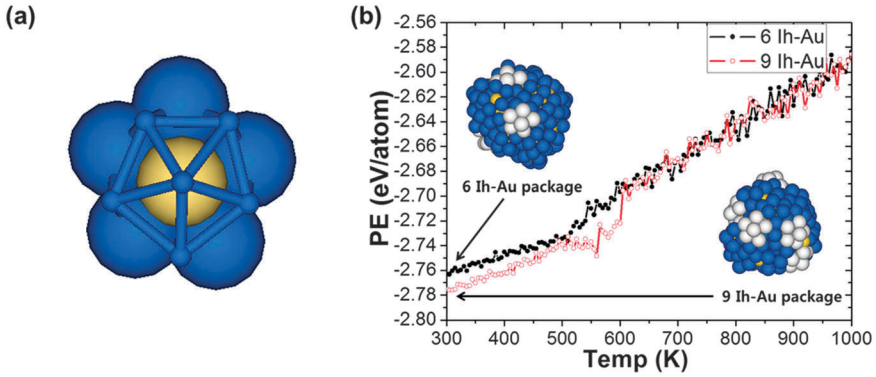

Fig. 3 (a) A perspective view of an Ih structure with a Au atom embedded in the Ih structure (that is, the Ih-Au structure): Au atoms are yellow, and blue atoms are Ag atoms of the Ih structure. (b) The results of the simulated annealing in the Ag90Au10 composition are compared with the number (nine *vs.* six) of Ih-Au packages on the surface; white atoms are the Ag atoms of the Ih-Au structure; the black dotted line indicates the structure with six Ih-Au packages; and the red circled line indicates the structure with nine Ih-Au packages on the surface.

Au nanoparticles of up to 135 atoms (1.5 nm size). Consequently, the current result for the pure Ag nanoparticles (Ih) is consistent with the results of earlier reports.

For the Type 1 compositions (Ag90Au10, Ag80Au20, and Ag70Au30), the Au solute atoms were combined with the Ih structure at the surface, giving rise to Ih-Au packages. One Ih-Au package comprises six Ag atoms surrounding one Au atom embedded at the center. Fig. 3(a) shows the configuration of the Ih-Au package, revealing a five-fold symmetry. Structurally, the Ih-Au package is mostly stable. Kim *et al.* showed that the internal atomistic configuration of Ag–Pd bimetallic nanoparticles can also be affected by the surface morphology of the cluster.[52] In the current study, the Ih-Au package was observed to form on the surface in the wide transition (liquid plus solid) region in the Ag-rich compositions. As a result, the Ag–Au bimetallic nanoparticles maintained the pre-formed surface morphology of the Ih-Au packages during solidification, and it appears that the formation of a crystalline structure was not favored at room temperature. This behavior explains why the formation of an amorphous structure is likely during the final solidification of the Ag-rich compositions.

To identify the structural stability of locally stable structures, we compared the energetic stability as a function of the number of Ih-Au packages on the surface for the same composition. We modeled an Ag90Au10 nanoparticle that can acquire either nine Ih-Au packages or six Ih-Au packages on its surface (see Fig. 3(b)). Then, we performed simulated annealing from 300 K to 1000 K. The initial structural energy in the case of nine Ih-Au packages (approximately +3.3 eV) was lower than that with six Ih-Au packages, which implies that the former structure is more stable than the latter.

In this way, we calculated the exact transition temperatures for Ag–Au bimetallic nanoparticles, which are shown in a nano phase diagram in Fig. 4. This phase diagram exhibits a complete solid-solution behavior similar to the bulk phase diagram, but the details are quite different. As expected, the freezing temperature is lower than that of the bulk state in every composition, which is a well-known property of nano-sized materials. We deduced that the wide transition region (40 K to 105 K) in the Ag-rich compositions could be attributed to the existence of locally stable Ih packages that were pre-formed at

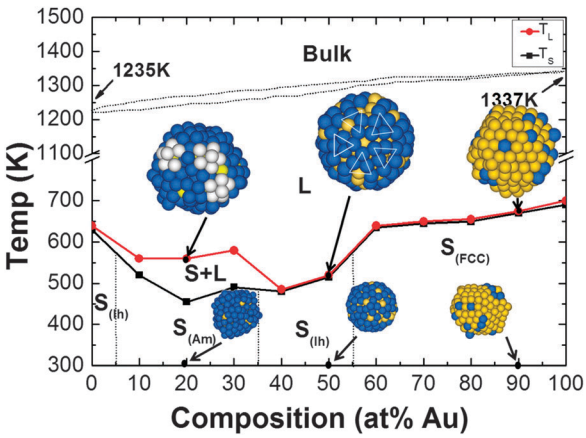

Fig. 4 Phase diagram of the Ag–Au bimetallic nanoparticles (270 atoms, 2 nm size). The red line (T_L) represents the surface freezing temperature, and the black line (T_S) represents the full freezing temperature. Atomistic configurations inside the diagram represent typical structures obtained at the given temperatures. Blue atoms indicate Ag atoms, and yellow ones are Au while white atoms are the Ag atoms of the Ih-Au package at the surface.

the surface before the final solidification. This pre-formation hinders the final positioning of the remaining atoms; consequently, the final solidification occurred at lower temperatures than that of the Au-rich compositions. In this way, the structure of the solid-state Ag–Au nanoparticles changed in relation to the Au composition, and it can be divided into three different phases (one phase is repeated): the Ih, amorphous (Am), Ih and FCC types.

The phase diagram of the Ag–Au nanoparticles cannot be compared directly with the bulk phase diagram.[26,27,31] The meaning of the solidus temperature line in the nano phase diagram, which corresponds to the full freezing temperature, is the same as that of the bulk system. However, the liquidus line of the bulk phase diagram refers to the temperature at which the liquid and solid phases are in a thermodynamic equilibrium state and coexist, whereas the liquidus line of the nano phase diagram refers to the starting temperature at which the surface of the local area is solidified. Surface freezing is also observed in the bulk system. Hence, in a pure composition

(100 at% Ag or 100 at% Au), the two lines that represent the solidus and liquidus of the bulk phase diagram are joined at one point; however, those two lines are not equal in the nano phase diagram. In a nano-sized system, the atomic properties differ between the surface and the interior. This difference is an important factor that determines the properties of nanoparticles; thus, surface freezing is a meaningful phenomenon that mainly affects the phase transition of nanoparticles. We define the surface freezing temperature as the temperature at which the nanoparticle begins to solidify; it is represented as the liquidus temperature line in the nano phase diagram. Then, we defined the phase transition region as the temperature range between the surface freezing temperature and the full freezing temperature.

It is well known that there is a hysteresis between the melting and freezing temperatures.[38,39,53] The hysteresis gap is quite large for the nanoparticles and it can be as large as 100 K or more. In this study, we investigated the phase transition only in the cooling process by using the simulated annealing method. For the heating process, the melting temperature regions were dependent on the initial configuration of bimetallic nanoparticles, and it is difficult to obtain exactly the phase transition temperature region by the simulated annealing method. One final caution is needed, however, because of the methodological incompleteness of the many-body force field model used in this study.

Summary

We constructed a phase diagram of 2 nm Ag–Au nanoparticles over the entire composition range by MD simulation combined with the use of the caloric curve, and MSD and SD analysis methods. The freezing temperature is lower than that of the bulk state by several hundred degrees for all compositions. The overall shapes of the nano phase diagrams are similar to those of the bulk phase diagrams of the Ag–Au bimetallic nanoparticles, in that the system behaves as a complete solid-solution.

In the bulk state, the phase diagram of the Ag–Au system is entirely a solid–solution diagram; accordingly, there is no additional phase below the solidus line, except for the stable single solid solution phase. However, the morphology of the solid-state Ag–Au nanoparticles in this study changed, and stable solid structures are proposed in relation to the Au composition as follows: Ih, amorphous, Ih and FCC.

Acknowledgements

This work was supported by the National Research Foundation of Korea (NRF) grant funded by the Korea government (MEST) (No. 2011-0028612).

References

1 R. Ferrando, J. Jellinek and R. L. Johnston, *Chem. Rev.*, 2008, **108**, 845–910.
2 J. H. Sinfelt, *J. Catal.*, 1973, **29**, 308–315.
3 N. Toshima and T. Yonezawa, *New J. Chem.*, 1998, **22**, 1179–1201.
4 R. Narayanan and M. A. El-Sayed, *Nano Lett.*, 2004, **4**, 1343–1348.
5 B. Lim, M. J. Jiang, P. H. C. Camargo, E. C. Cho, J. Tao, X. M. Lu, Y. M. Zhu and Y. A. Xia, *Science*, 2009, **324**, 1302–1305.
6 J. G. Lee, H. Mori and H. Yasuda, *Phys. Rev. B: Condens. Matter*, 2002, **65**, 132106.
7 W. D. King, J. D. Corn, O. J. Murphy, D. L. Boxall, E. A. Kenik, K. C. Kwiatkowski, S. R. Stock and C. M. Lukehart, *J. Phys. Chem. B*, 2003, **107**, 5467–5474.
8 L. J. Lewis, P. Jensen and J.-L. Barrat, *Phys. Rev. B: Condens. Matter*, 1997, **56**, 2248.
9 M. Schmidt, R. Kusche, B. von Issendorff and H. Haberland, *Nature*, 1998, **393**, 238–240.
10 S. Sankaranarayanan, V. R. Bhethanabotla and B. Joseph, *Phys. Rev. B: Condens. Matter*, 2006, **74**, 155441.
11 B. Karthikeyan, M. Anija and R. Philip, *Appl. Phys. Lett.*, 2006, **88**, 053104.
12 M. P. Murray-Methot, M. Ratel and J. F. Masson, *J. Phys. Chem. C*, 2010, **114**, 8268–8275.
13 B. Rodriguez-Gonzalez, A. Burrows, M. Watanabe, C. J. Kiely and L. M. Liz-Marzan, *J. Mater. Chem.*, 2005, **15**, 1755–1759.
14 A. Q. Wang, Y. Hsieh, Y. F. Chen and C. Y. Mou, *J. Catal.*, 2006, **237**, 197–206.
15 K. H. Park, S. Kim, S. M. Yang and H. G. Park, *J. Nanosci. Nanotechnol.*, 2009, **9**, 1374–1378.
16 S. Tokonami, N. Morita, K. Takasaki and N. Toshima, *J. Phys. Chem. C*, 2010, **114**, 10336–10341.
17 S. C. Tang, S. Vongehr and X. K. Meng, *J. Mater. Chem.*, 2010, **20**, 5436–5445.
18 M. Haruta, T. Kobayashi, H. Sano and N. Yamada, *Chem. Lett.*, 1987, 405–408.
19 S. Carrettin, P. McMorn, P. Johnston, K. Griffin and G. J. Hutchings, *Chem. Commun.*, 2002, 696–697.
20 Y. Iizuka, A. Kawamoto, K. Akita, M. Date, S. Tsubota, M. Okumura and M. Haruta, *Catal. Lett.*, 2004, **97**, 203–208.
21 Y. Iizuka, T. Miyamae, T. Miura, M. Okumura, M. Date and M. Haruta, *J. Catal.*, 2009, **262**, 280–286.
22 A. Q. Wang, C. M. Chang and C. Y. Mou, *J. Phys. Chem. B*, 2005, **109**, 18860–18867.
23 C. W. Yen, M. L. Lin, A. Q. Wang, S. A. Chen, J. M. Chen and C. Y. Mou, *J. Phys. Chem. C*, 2009, **113**, 17831–17839.
24 A. Sandoval, A. Aguilar, C. Louis, A. Traverse and R. Zanella, *J. Catal.*, 2011, **281**, 40–49.
25 A. Q. Wang, J. H. Liu, S. D. Lin, T. S. Lin and C. Y. Mou, *J. Catal.*, 2005, **233**, 186–197.
26 D. H. Kim, H. Y. Kim, J. H. Ryu and H. M. Lee, *Phys. Chem. Chem. Phys.*, 2009, **11**, 5079–5085.
27 H. Y. Kim, D. H. Kim and H. M. Lee, *J. Nanosci. Nanotechnol.*, 2011, **11**, 2251–2255.
28 J. Park and J. Lee, *CALPHAD: Comput. Coupling Phase Diagrams Thermochem.*, 2008, **32**, 135–141.
29 T. Tanaka and S. Hara, *Z. Metallkd.*, 2001, **92**, 467–472.
30 J. Lee, T. Tanaka and H. Mori, *CALPHAD: Comput. Coupling Phase Diagrams Thermochem.*, 2007, **31**, 105–111.
31 D. H. Kim, H. Y. Kim, H. G. Kim, J. H. Ryu and H. M. Lee, *J. Phys.: Condens. Matter*, 2008, **20**, 035208.
32 Rifkin, The center for simulation, University of Connecticut, http://xmd.sourceforge.net.
33 G. J. Martyna, M. L. Klein and M. Tuckerman, *J. Chem. Phys.*, 1992, **97**, 2635–2643.
34 Y. K. T. Cagin, Y. Qi, H. Ikeda, W. L. Johnson and W. A. Goddard III, *Mater. Res. Soc. Symp. Proc.*, 1999, **554**, 43.
35 Y. Qi, T. Cagin, Y. Kimura and W. A. Goddard, *J. Comput.-Aided Mater. Des.*, 2002, **8**, 233–243.
36 Y. Qi, T. Cagin, Y. Kimura and W. A. Goddard, *Phys. Rev. B: Condens. Matter*, 1999, **59**, 3527–3533.
37 C. W. Gear, *Numerical Initial Value Problems in Ordinary Differential Equations*, Prentice-Hall, Englewood Cliffs, NJ, 1971, ch. 9.
38 G. Rossi and R. Ferrando, *Nanotechnology*, 2007, **18**, 225706.
39 Y. Shibuta and T. Suzuki, *Chem. Phys. Lett.*, 2011, **502**, 82–86.
40 P. Jalali and M. Li, *Phys. Rev. B: Condens. Matter*, 2005, **71**, 014206.
41 J. H. Ryu, H. Y. Kim, D. H. Kim, D. H. Seo and H. M. Lee, *J. Phys. Chem. C*, 2010, **114**, 2022–2026.
42 D. H. Seo, H. Y. Kim, J. H. Ryu and H. M. Lee, *J. Phys. Chem. C*, 2009, **113**, 10416–10421.

43 A. Morita, *J. Phys. A: Math. Gen.*, 1996, **29**, 6525–6529.
44 L. M. Wang, Z. J. Li, Z. M. Chen, Y. Zhao, R. P. Liu and Y. J. Tian, *J. Phys. Chem. B*, 2010, **114**, 12080–12084.
45 H. J. Lee, T. Cagin, W. L. Johnson and W. A. Goddard, *J. Chem. Phys.*, 2003, **119**, 9858–9870.
46 J. H. Ryu, H. Y. Kim, D. H. Kim, S. K. Choi and H. M. Lee, *J. Nanosci. Nanotechnol.*, 2009, **9**, 2553–2557.
47 D. Reinhard, B. D. Hall, D. Ugarte and R. Monot, *Phys. Rev. B: Condens. Matter*, 1997, **55**, 7868–7881.
48 F. Baletto and R. Ferrando, *Rev. Mod. Phys.*, 2005, **77**, 371–423.
49 H. S. Nam, N. M. Hwang, B. D. Yu, D. Y. Kim and J. K. Yoon, *Phys. Rev. B: Condens. Matter*, 2005, **71**, 233401.
50 H. S. Nam, N. M. Hwang, B. D. Yu and J. K. Yoon, *Phys. Rev. Lett.*, 2002, **89**, 275502.
51 F. Baletto and R. Ferrando, *Rev. Mod. Phys.*, 2005, **77**, 371–423.
52 H. Y. Kim, H. G. Kim, J. H. Ryu and H. M. Lee, *Phys. Rev. B: Condens. Matter*, 2007, **75**, 212105.
53 Y. Shibuta and T. Suzuki, *J. Chem. Phys.*, 2008, **129**, 144102.

